Springer

Journal of
Mechanical
Science and
Technology

Journal of Mechanical Science and Technology 22 (2008) 914~923

www.springerlink.com/content/1738-494x

Dynamic cutting force on-line estimation using a 4-electrode cylindrical capacitive displacement sensor mounted on a high speed milling spindle

Il-Hae Kim*

Camsys Co., Dasan 007, 172 Gongreung 2-dong, Nowon-gu, Seoul, 139-743, South Korea

(Manuscript Received December 26, 2007; Revised January 15, 2008; Accepted February 22, 2008)

Abstract

In this paper, a 4-electrode cylindrical capacitance displacement sensor (CCDS) is presented as an indirect force sensor for a high speed milling spindle. A rotor-bar system for the magnetic exciter is designed to investigate the tool deflection with respect to the applied cutting force. To extract the deflection signal from the CCDS, the dynamic orbital motion at each rotating speed of spindle is predetermined and then subtracted from the CCDS signal. The CCDS signal is also used as a reference sync signal. The rotor-bar system is designed so that the rotor affects the tool-spindle dynamics only as an added mass but does not contribute to the bending property. The additional effect of the rotor mass in the exciter setup is compensated for by an experimental modeling. The cutting force can be estimated by using modified CCDS signals and FRF. Cutting experiments are conducted to show reliable performances of the proposed approach by high speed machining applications.

Keywords: Cutting force online measurement; 4-electrode cylindrical capacitive displacement sensor (CCDS); High speed milling spindle

1. Introduction

The monitoring of machining conditions has been an attractive research object for many decades. However, providing practical and reliable monitoring solutions is still a demanding task for milling machines with high speed spindles. The sensors for vibrations and cutting forces have to be reasonably sensitive over a broad bandwidth of cutting dynamics, because the amplitudes of cutting force changes according to cutting condition variations are quite small under the conditions of high cutting speeds and small depths of cut. And the deflection of the tool-spindle system has to be investigated if the indirect displacement measurement at the spindle is to be used.

Table type dynamometers have been standards for long time; however, they are not adequate for high speed machining. With the additional mass of the workpiece, the lowered natural frequency of the dynamometer setup could distort the cutting dynamics [1, 2]. Tounsi and Otho [3] proposed an accelerometer-based method to compensate for the responses of the dynamometer at high frequencies. Six accelerometers were installed to model the dynamics of the dynamometer at which the workpiece was directly attached. Their scheme exhibited accurate measurements up to 2kHz. Indirect cutting force measurement methods were also proposed using various signals such as motor currents or acoustic emissions of cutting conditions, and other devices like strain gauge type dynamometers, etc. [4-6]. But the signal bandwidths of these methods are usually too low or limited to cover the conditions of high speed machining. Recently, Albrecht et al. [7] proposed a cutting force measurement scheme using a probe type gap sensor at a spindle, in which the cutting dynamics up to 1 kHz could be measured with a modified FRF with Kalman filter.

In this study, a 4-electrode CCDS mounted at the

*Corresponding author. Tel.: +82 2 970 6475, Fax.: +82 2 971 6475
E-mail address: chyarlie@gmail.com
DOI 10.1007/s12206-008-0214-2

spindle is proposed as an indirect cutting force sensor via sensing the spindle displacements by high speed milling. Previously, the displacement measurement by the CCDS has been applied successfully for an in-process monitoring of various machining conditions such as tool wear, cutting vibration, and surface roughness [8-10]. To build an indirect force measuring system using the CCDS at the spindle, a reasonable method for extraction of the pure spindle deflection signals due to cutting forces is investigated. To acquire the tool point FRF of the tool-spindle system under cutting force excitation with frequencies up to 2 kHz, a non-contact type magnetic exciter and a rotor-bar system is manufactured and applied. To calibrate the relation between the spindle deflection and the cutting forces, a reliable tool dynamometer is installed beneath the exciter setup, and the signals for various rotating speeds and exciting forces are compared.

2. Cutting force estimation and validation system configuration

If the dynamic characteristics of a tool-spindle system were invariant for various operating conditions, the cutting force could be simply obtained by identifying the deflection and the stiffness of the system. For high-speed operation, however, both the spindle error motion and the tool point FRF of the tool-spindle system depend on the rotating speed. To build an accurate cutting force estimation system, the varying properties with rotating speed should be identified at each speed range. Fig. 1 illustrates all the necessary devices for the FRF identification and the cutting force estimation system. It has been previously demonstrated that the CCDS is better at eliminating geometric error components of a rotor than other probe type sensors [10, 11]. The CCDS has an inner diameter of 63.8 mm, nominal gap of 150μm, and sensitivity of 3.35μm/V at working ranges of ±30μm in x- and y-directions. The sensor output is monitored on a personal computer for further signal processing. Once the tool-spindle dynamics is identified, only the CCDS at the spindle is required as hardware to estimate the cutting force.

The magnetic exciter equipped with another CCDS is for generating the cutting force to the tool-spindle system in non-contact condition over the whole operating speed range. Rantatalo et al. [12] proposed a similar configuration using non-contact spindle excitations with inductive displacement measurements at exciter position to identify the spindle dynamics up to 2kHz. The configuration in Fig. 1 is the same one used in [13] except for the tool holder and the rotor-bar system which interacts with the magnetic exciter. The exciter has 8 poles and 84 coil turns for each pole. The bias current is 0.4A and the force it can generates is 150N in RMS. The maximum exciting frequency is 2kHz. The force output was verified by using the test rig in [14]. In previous research, a cylindrical part was directly attached to the spindle and the spindle dynamics up to 1kHz was measured. In this paper, the rotor-bar system is adopted to represent the actual tool-spindle configuration for machining operation during the FRF identification procedure. The bar is designed to have the same dynamic properties of the end mills used in the cutting experiments. The applied force is also measured by the 9257B Kistler dynamometer installed beneath the exciter.

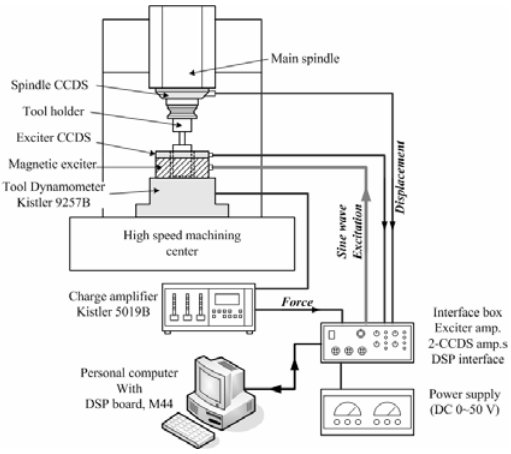

Fig. 1. Overall system configuration for cutting force estimation and validation.

3. Identification of the spindle deflection due to the cutting force

The displacement by the CCDS contains not only the pure deflection by the cutting force but also the spindle error motion. This spindle error motion is the dynamic additional motion according to the spindle characteristics. The thermal and mechanical behavior of high-speed spindles is difficult to predict because of the complicated nature of the heat generation and heat transfer in a motorized spindle system [15]. The bearing configuration, the centrifugal force of the

spindle shaft, and thermally induced preloads are affecting the system response while increasing the operating speed [15, 16]. Fig. 2 shows the typical additional dynamic motions of a high-speed spindle itself measured by the CCDS.

The trace at top left corner represents a spindle error motion during a single revolution. Other traces show the movement of this spindle error motion. The size of the spindle error motion increased with increasing spindle speed. However, the shapes and sizes stayed unchanged if the rotating speed was kept unchanged. Hence, the spindle error motion due to the characteristics of the spindle can be predetermined at each rotating speed. The center of the spindle error motion wandered for some periods after the spindle started to rotate, but soon came to steady state. It took about 40 seconds at 12,500rpm and 90 seconds at 15,000rpm. Programmed delay is recommended before the tool is engaged with the workpiece. The spindle error motions are stored after this transient period and when the spindle becomes thermally balanced. This motion will be referred as an intrinsic spindle error motion.

The deflections induced by cutting forces can be obtained by subtracting the superposed intrinsic spindle error motions from the measured displacements data. For the subtraction, the two signals should be synchronized. The CCDS signal itself is used as a reference for the synchronization. If any slight mis-

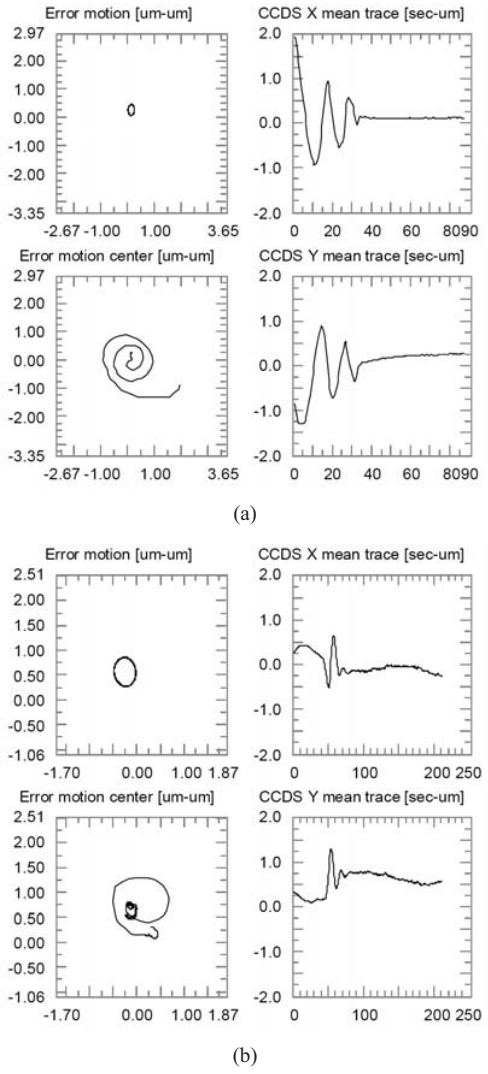

Fig. 2. Intrinsic dynamic motion of a spindle itself from stop to steady state condition: (a) 12,500rpm (b) 15,000rpm.

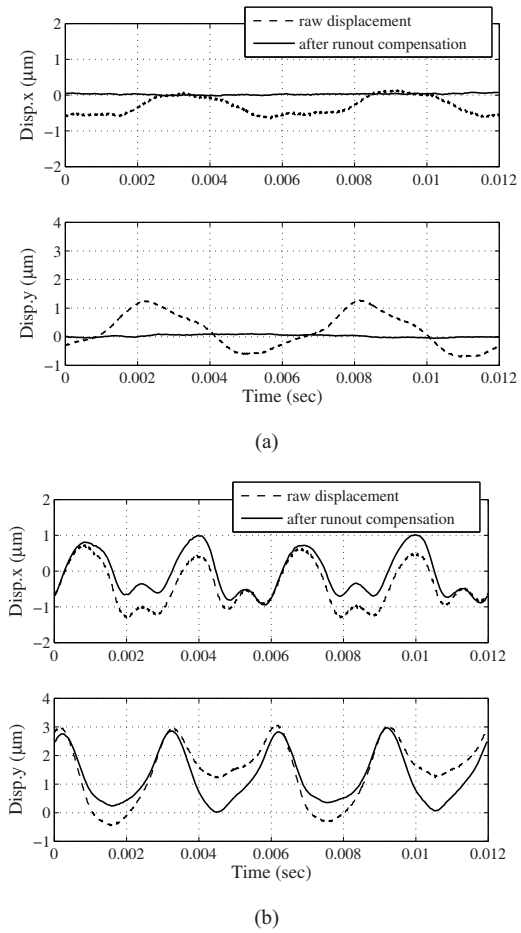

Fig. 3. Displacement signals before and after intrinsic spindle error motion compensation; two spindle revolutions are shown: (a) free run (air cutting) (b) cutting.

alignment of the tool is negligible, the first harmonic component in cutting force signal, which corresponds to the rotating speed, would be small. Then, the cutting force would have little effect on the first harmonic component of the intrinsic spindle error motion. Those first harmonic components of the measured and the stored data are synchronized to cancel out the phase difference. The deflection related only to the cutting force is now obtained as in Eq. (1).

$$X(\omega) = X_c(\omega) - X_i(\omega)\exp\left[j(\phi_i^{(1)} - \phi_c^{(1)})\omega/\omega^{(1)} \right] \quad (1)$$

Here, X_c (ω) and X_i (ω) are the discrete Fourier transform (DFT) of the uncompensated spindle error motion during cutting process and the pre-acquired intrinsic spindle error motion. $\phi_c{}^{(1)}$ and $\phi_i{}^{(1)}$ are the phases of the first harmonic component of each signal. $\omega^{(1)}$ is the frequency of the first harmonics. Fig. 3 shows the spindle displacement data before and after the intrinsic spindle error motion compensation.

4. Identification of the tool point frequency response function (FRF) between the deflection and the applied force

4.1 Rotor-bar system for experimental modeling of a cutting tool

Fig. 4 shows the rotor-bar system which is used for the tool point FRF identification procedure. It is designed so that the rotor plays only as an added mass and not to contribute to the bending property of the tool-spindle system. The bending diameter will have the same value as the tool used in experiments, so the deflection characteristics of the tool-spindle due to the applied cutting force can be investigated. It will show the same dynamic characteristics if we can remove the added mass effect of the rotor. The relation between the exerted force at the cutting point and the measured displacement at the CCDS is investigated during the magnetic excitation experiments. Responses at the rotor-CCDS are also investigated along with the responses at the spindle-CCDS.

To minimize the mass of the rotor, the body of the rotor is made of duralumin, and then silicon steel sheets of thickness 0.5mm are stacked around the body. It is secured by a power lock to a bar of diameter 10mm which is made of the same material and size as the tool. The rotor is balanced to less than 0.1 g·mm. This setup is attached to the spindle by the collet chuck in the same way that the tool is installed. Except the rotor at the cutting point, the rotor-bar system can represent the actual tool-spindle dynamics

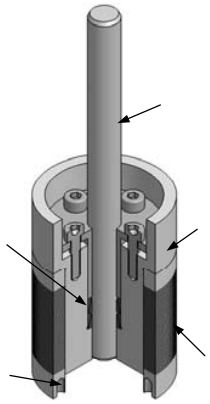

(a)

(b)

Fig. 4. Rotor-bar system for magnetic excitation: (a) schematic of the rotor-bar (b) photo of installed rotor-bar system at spindle.

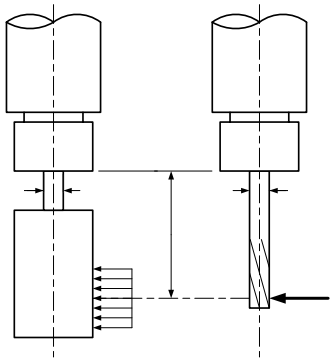

Fig. 5. Configurations for exciting tests using the magnetic exciter and an impulse hammer.

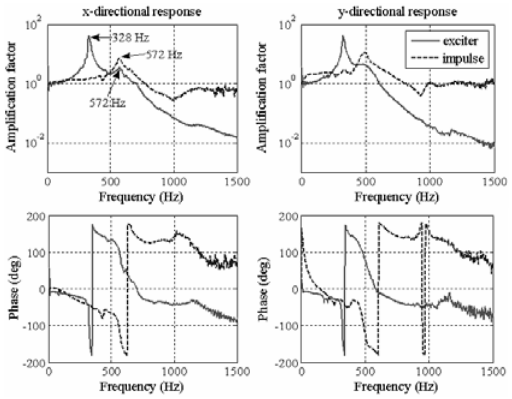

Fig. 6. Comparison of excitation result with an impulse test result (stationary spindle, response by the CCDS at the spindle).

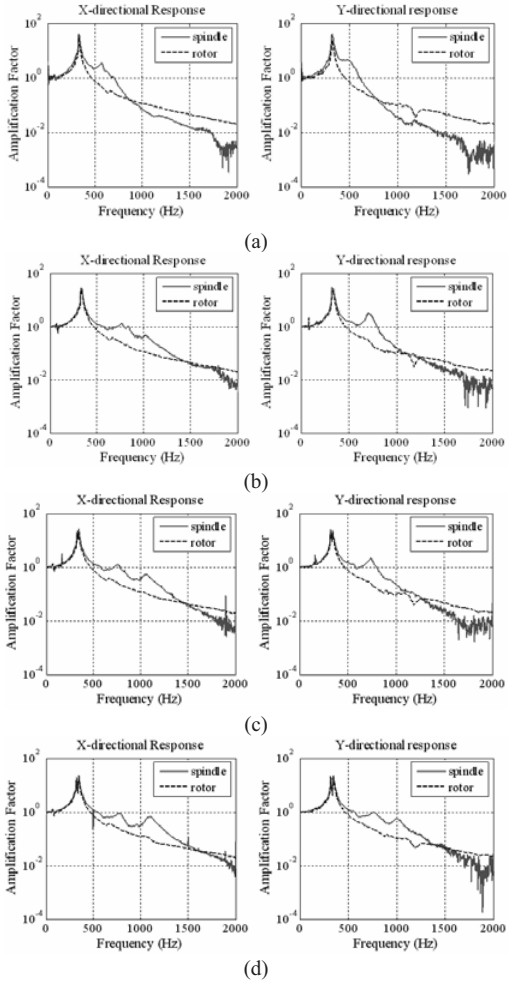

Fig. 7. Frequency responses of spindle and rotor at various spindle speeds: (a) stationary spindle (b) 5,000rpm (c) 10,000rpm (d) 15,000rpm.

including the shear deformation of the cutting tool.

4.2 Measurement of the FRF

Excitation experiments were performed with frequencies from 0 to 2kHz by 4Hz increment. First, the excitation response of the stationary spindle is compared with the one by a typical impact test. In this paper, the spindle at 200 rpm is referred to as the stationary spindle. As an excitation input, a single frequency sinusoidal waveform is applied as shown in Fig. 5.

Fig. 6 shows the normalized FRFs of the spindle displacement by dividing the measured response with a static response. Because of the additional mass effect of the rotor, the first mode at 328Hz dominates in the response. This effect has to be compensated for to get the correct tool point FRF.

Displacement responses at the rotor and the spindle are shown in Fig. 7. It can be observed that the response of the rotor remains nearly invariant while that of the spindle shows different characteristics as the spindle speed increases. However, the displacement responses at the rotor and the spindle agree quite well in the range below 400Hz.

Fig. 8 shows more detailed views of the results. The noticeable difference in the response of the rotor is the split-up of the first natural frequency. This can be explained by the increasing gyroscopic moment of the rotor at high spindle speed. Similar results were reported in other researches [12, 16-18].

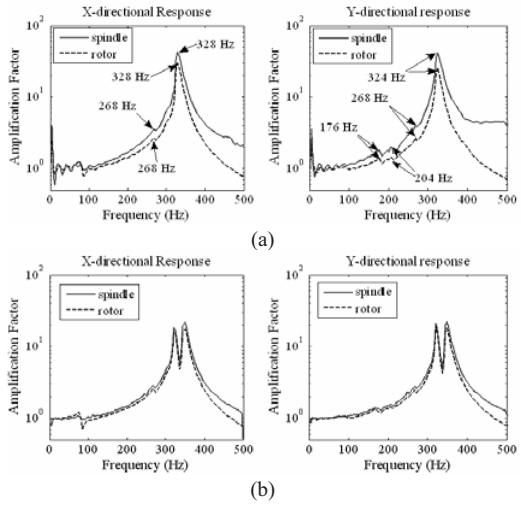

Fig. 8. Comparison of frequency response of spindle and rotor: (a) stationary spindle (b) 15,000rpm.

From the results of Figs. 6-8, we can conclude that the mode around 320 Hz is caused not by the spindle characteristics but by the additional rotor mass effects. A second order single degree-of-freedom system is assumed to model these phenomena. The FRF of the tool-spindle system with the rotor $H_{ms}(s)$ can be described as a multiplication of the approximated rotor function $\hat{H}_{rotor}$ and the tool-spindle system function without the rotor $H(s)$ as in Eq. (2).

$$H_{ms}(s) = \frac{b_1 s + b_2}{s^2 + a_1 s + a_2} H(s) = \hat{H}_{rotor}(s) H(s) \tag{2}$$

As both $H(s)$ and $H_{ms}(s)$ are normalized by the static responses, $H(0) = H_{ms}(0) = \hat{H}_{rotor} = 1$ if $s = j\omega = 0$, which makes $b_2 = a_2$. Then, coefficients a_1, a_2, b_1, b_2 can be determined by fitting this with the experimental FRF of the rotor-spindle system as in Eq. (3). The fitted coefficients are listed in Table 1. The fitted model for compensating the mass of the exciter rotor is plotted and compared with measured data in Fig. 9.

$$H_{ms}(\omega) = \frac{jb_1\omega + b_2}{-\omega^2 + ja_1\omega + a_2} H(\omega), \quad b_2 = a_2 \tag{3}$$

Then, the FRF of the spindle is compensated for as in Eq. (4). Δt is the time delay of 0.1287ms between the two responses and $\omega_c = 400\text{Hz} \simeq 2{,}513\text{rad/s}$. As can be seen in Fig. 8, the rotor also shows complex responses due to the gyroscopic moment at high rotating speed. These responses will not appear in an actual cutting experiment configuration. Hence, an empirical approach is taken to compensate for these responses of the rotor. Through extensive investigation of the experimental result, it is assumed that the nonlinear responses of the rotor appear mainly in frequency range below 400 Hz. So the FRF of the spindle in range below 400 Hz is compensated for with empirically obtained data. The reconstructed FRF through this procedure is demonstrated with the FRF before compensation and the result by impulse test in Fig. 10.

$$H(\omega) = \begin{cases} \dfrac{|\hat{H}_{rotor}(\omega)|}{|H_{rotor}(\omega)|} \cdot \hat{H}^{-1}_{rotor}(\omega) \cdot H_{ms}(\omega) \cdot e^{j\omega\Delta t}, & \omega \le \omega_c \\ \hat{H}^{-1}_{rotor}(\omega) \cdot H_{ms}(\omega) \cdot e^{j\omega\Delta t} & \omega \ge \omega_c \end{cases} \tag{4}$$

After the compensation of the attached rotor-bar system in the exciting experiments, the FRF of the tool-spindle system becomes similar in level to that of the impulse test. Conducting an impulse test is a simple procedure, but obtaining an accurate result at high frequency region is a demanding job. To identify the FRF of the high-speed spindle, non-contact magnetic exciting experiments are conducted on the rotating spindle.

Table 1. First modal parameters of the FRF of the rotor.

Parameter	X-directional	Y-directional
a_1	55.33	52.3
a_2 , b_2	4.40×10^6	4.28×10^6
b_1	122.02	76.55

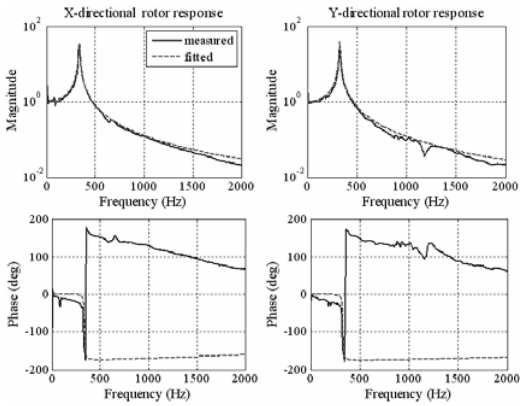

Fig. 9. FRF of rotor fitted into a 1-DOF vibration system.

4.3 Measurement of dynamic characteristics of the spindle

Excitation experiments were conducted by applying dynamic forces to the spindle with sinusoidal

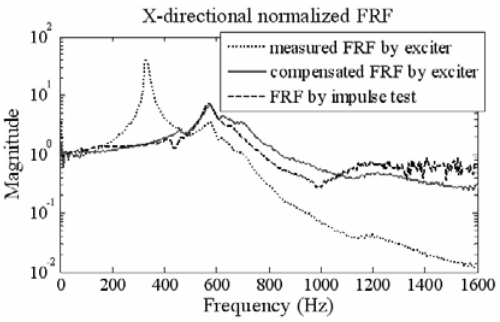

Fig. 10. Compensated FRF and FRF by impulse test at stationary state.

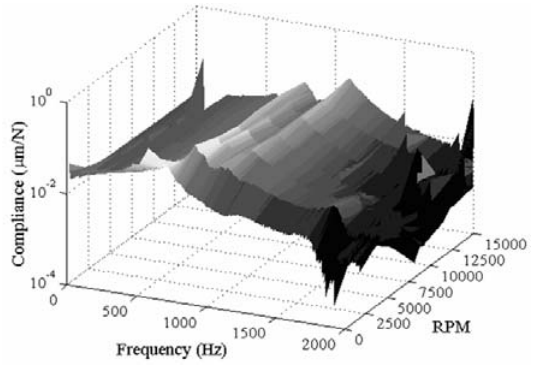

(a)

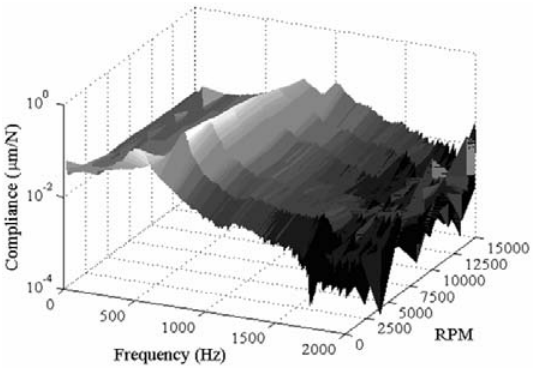

(b)

Fig. 11. Compliances of the spindle for various rotating speed and exciting frequencies: (a) *x*-directional compliance and (b) *y*-directional compliance.

excitation frequencies from 0 to 2kHz by 4Hz increment at each spindle speed from 2,500 to 15,000rpm by 2,500rpm incremental step. Fig. 11 shows the obtained FRFs (compliances) of the spindle. The magnitude of the driving force is kept constant at 10N so as to provide consistent driving amplitude over the whole range of driving frequencies. The spindle compliance above 800Hz is calculated from the input force, because the measured force signal can be erroneous due to the dynamic coupling between the exciter and the dynamometer. As mentioned earlier, the dynamic characteristics of a high-speed spindle are complex and the results can be regarded as characteristics of the given spindle under test.

The noise at very high frequency region can be explained by the small displacement response. As can be identified in Fig. 10, the measured raw FRF by the exciter is quite small in the high frequency region. The noise from the CCDS is also amplified during the FRF compensation and appears in the result. A smaller rotor for excitation target may help reduce this noise level. Increasing the amplitude of the exciting force is difficult because of the excessive response at resonance frequencies.

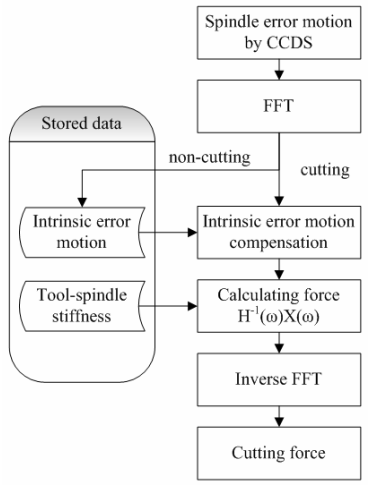

Fig. 12. Diagram of cutting force estimation system.

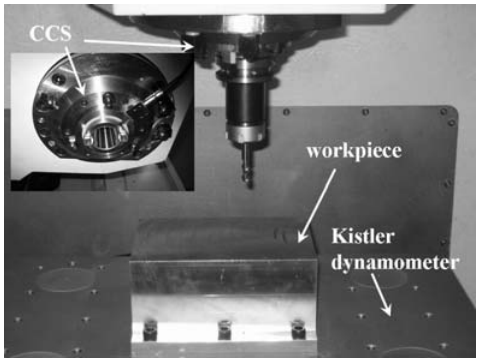

Fig. 13. Photo of the cutting force on-line estimation system.

A cutting force estimation scheme is shown in Fig. 12. First, the CCDS signal is FFT-transformed and then the intrinsic error motion is compensated. This cutting related signal is multiplied by the spindle stiffness to get the cutting force in frequency domain. Finally, the cutting force is obtained by inverse FFT.

5. Cutting test

5.1 Cutting test results

Cutting tests were conducted and the results from the CCDS and the dynamometer were compared. The workpiece material was NAK80 mold steel with

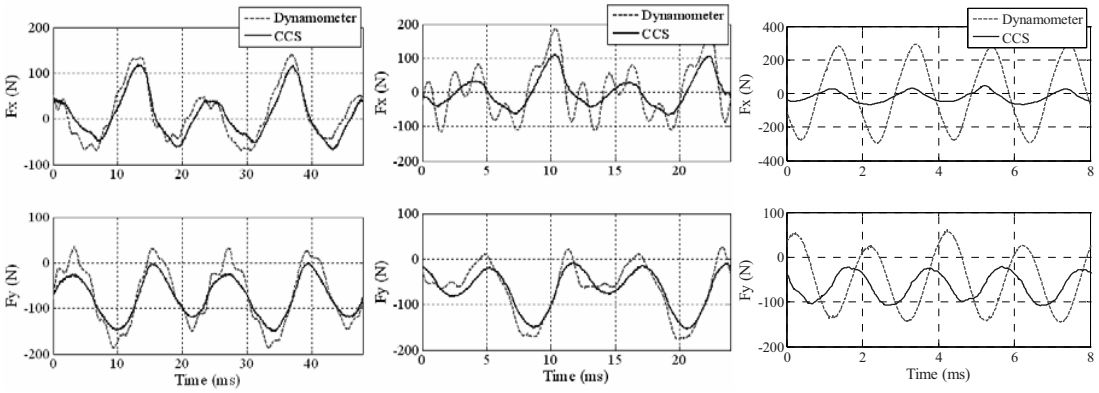

Fig. 14. Cutting test results (for down milling): (a) 2,500rpm (rotating frequency: 41.67Hz, dominant cutting frequency: 83.33 Hz) (b) 5,000rpm (rotating frequency: 83.33Hz, dominant cutting frequency: 166.67Hz) (c) 15,000rpm (rotating frequency: 250Hz, dominant cutting frequency: 500Hz)

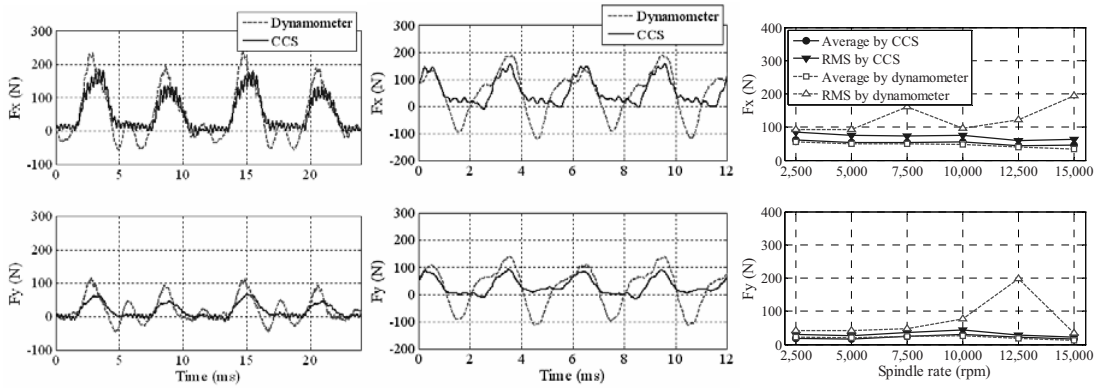

Fig. 15. Cutting test results: (a) 5,000rpm (b) 10,000rpm (c) variations of average and RMS of cutting force according to spindle rate.

hardness of 42 in Rockwell C scale. A two-fluted, 10 mm in diameter, TiAIN coated, tungsten carbide ball end mill with 30 degree of helix angle was used. Feed was set at 0.2mm/rev and depth of cut was set to 2 mm for radial and to 0.3mm for axial direction. Only the rotating speed was varied from 2,500 to 15,000 rpm because the dynamics change due to the rotating speed is of interest. The experimental setup for this cutting test is shown in Fig. 13.

Fig. 14 shows the comparison results of the dynamometer and the CCDS system. The cutting force estimated by the CCDS agrees well with the measured force by the dynamometer at slow rotating speed. However, fluctuation of high frequency components becomes bigger in dynamometer data as the rotating speed increases. This is obviously due to the low bandwidth of the dynamometer setup. An impact test on this setup identifies that the first resonances occur at 500Hz in *x*- and 450Hz in *y*-direction.

Side cutting experiments were also conducted with SM45C in up-milling mode. A two-fluted, 10mm in diameter, TiAIN coated, tungsten carbide flat end mill with 30 degree of helix angle was used. Feed was set at 0.2mm/rev and depth of cut was set to 0.3mm for radial and to 10mm for axial direction. Fig. 15 shows the sample data at 5,000rpm and 10,000rpm.

High frequency vibration can be monitored in data by the CCDS as shown in Fig. 14 (a). With the tool passing frequency of 166.67Hz, small chattering with frequency of 3.3kHz can be detected by the CCDS. This frequency corresponds to the 6th mode of the tool-spindle system.

In Figs. 14 and 15, other cutting parameters were kept the same, which means the amount of material removed was the same. At higher machining speed, the cutting force usually decreases because of thermal softening [19]. As can be seen in Fig. 16 (c), the estimated cutting force agrees well with this statement, but the signal from the dynamometer does not due to resonance between the dominant cutting frequency and the first natural frequency of the dynamometer setup.

5.2 Remarks on performance

The resolution and the range of cutting force by this method rely on the displacement sensor. The CCDS usually shows a noise level about 3mV. To include the effect from other error sources, such as an error in the FRF measurement at high frequency, a bigger noise level is assumed. If a noise level is assumed to be 10mV, the displacement resolution becomes 33.5nm as the sensor gain is 3.35μm/V. The approximate value of the static compliance between displacement and force is measured to be 0.015μm/N. Thus, a 10mV resolution in the displacement becomes 2.23N resolution in cutting force. Likewise, the measurable range of cutting force is ±2kN in ±30μm range of the CCDS, which is beyond feasible limits. Next, the size error of the target due to thermal deformation can cause a gain error. If there is a temperature difference of 8.8℃ between the target and the CCDS, the sensor gap will change by 3μm and the displacement sensor will have 4 percent gain error, which is calculated in a similar way as in [7] with the specifications of the 4-electrode CCDS in this paper.

6. Conclusion

An on-line cutting force estimation system for a milling with a high-speed spindle is developed and experimentally validated, which uses a 4-electrode CCDS at the spindle and a rotor-bar system in the tool point FRF identification procedure. An empirical method to compensate for the complex nature of the spindle error motion and the tool-spindle dynamics is proposed. To extract displacement signals related only to the cutting force, the intrinsic spindle error motions at each rotating speed are pre-acquired and then compensated for by using its own signal as a sync trigger. As the dynamics of a high-speed spindle is complex and an analytic solution is hard to get, the dynamic characteristics of the spindle-tool system are experimentally identified up to 2kHz with a non-contact magnetic exciter with a built-in CCDS. The dynamics of this setup differs from that of the cutting setup because a rotor for the magnetic exciter is inevitable. So the additional mass effect of this rotor is compensated for by modeling it as a single degree-of-freedom system of second order. The estimated force was compared with the cutting force measured by the dynamometer. The results demonstrate the effectiveness of the proposed method. The cutting dynamics over a wide bandwidth can be monitored successfully by using the CCDS which is built into the spindle housing.

Acknowledgments

This work was partially supported by the Industrial Technology Development Program of the Ministry of Commerce, Industry and Energy (MOCIE) under “Development of a machining center for IT part machining with a nano-spindle” project.

References

[1] Y. L. Chung and S. A. Speiwak, A model of high performance dynamometer, *ASME Trans. J. Eng. Ind.,* 116 (1994) 279-288.

[2] S. Auchet, P. Chevrier, M. Lacour and P. Lipinski, A new method of cutting force measurement based on command voltages of active electro-magnetic bearings, *Int. J. Machine Tools Manufact.,* 44 (2004) 1441-1449.

[3] N. Tounsi and A. Otho, Dynamic cutting force measuring, *Int. J. Machine Tools Manufact.,* 40 (2000) 1157-1170.

[4] D. W. Cho, S. J. Lee and C. N. Chu, The state of machining process monitoring research in Korea, *Int. J. Machine Tools Manufact.,* 39 (11) (1999) 1697-1715.

[5] B. Sick, On-line and indirect tool wear monitoring in turning with artificial neural networks: A review of more than a decade of research, *Mech. Sys. Sig. Proc.,* 16 (4) (2002) 487-546.

[6] M. B. Jun, O. B, Ozdoganlar, R. E. DeVor and S. G. Kappor, A. Kirchheim and G. Schaffner, Evaluation of a spindle-based force sensor for monitoring and fault diagnosis of machining operations, *Int. J. Machine Tools Manufact.,* 42 (2002) 741-751.

[7] A. Albrecht, S. S. Park, Y. Altintas and G.

Pritschow, High frequency bandwidth cutting force measurement in milling using capacitance displacement sensors, *Int. J. Machine Tools Manufact.,* 45 (2005) 993-1008.

[8] I. H. Kim, D. Y. Jang, W. J. Kim and D. C. Han, In-process sensing of tool wear and process states using a cylindrical displacement sensor in hard turning, *Proc. IMechE Part B: J. Eng. Manuf.,* 215 (12) (2001) 1673-1682.

[9] I. H. Kim and D. Y. Jang, Cutting vibration monitoring using a spindle displacement sensor in turning, Proc. of DETC'03, ASME 2003 Design Engineering Technical Conferences and Computers and Information in Engineering Conference, Chicago, Illinois, USA. (2003).

[10] H. K. Chang, J. H. Kim, I. H. Kim, D. Y. Jang and D. C. Han, In-process surface roughness prediction using displacement signals from spindle motion, *Int. J. Machine Tools Manufact.,* 47 (2007) 1021-1026.

[11] H. J. Ahn, S. Jeon and D. C. Han, Error analysis of the cylindrical capacitive sensor for active magnetic bearing spindles, *ASME Trans. J. Dyn. Sys. Meas. Control,* 122 (2000) 102-107.

[12] M. Rantatalo, J. O. Aidanpää, B. Böransson and P. Normann, Milling machine spindle analysis using FEM and non-contact spindle excitation and response measurement, *Int. J. Machine Tools Manufact.,* 47 (2007) 1034-1045.

[13] J. H. Kim, H. K. Chang, D. C. Han, D. Y. Jang and S. I. Oh, Cutting force estimation by measuring spindle displacement in milling process, *CIRP Ann. Manuf. Technol.,* 54 (1) (2005) 67-70

[14] H. J. Ahn, J. H. Kim, J. J. Lee, J. H. Kim, D. Y. Jang and D. C. Han, Speed-dependent tool tip compliance measurement of a high-speed machine tool spindle using an active magnetic bearing, IEEE/ ASME International Conference on Advanced Intelligent Mechatronics, Monterey, California, USA. (2005).

[15] C. W. Lin, J. F. Tu and J. Kamman, An integrated thermo-mechanical-dynamic model to characterize motorized machine tool spindles during very high speed rotation, *Int. J. Machine Tools Manufact.,* 43 (2003) 1035-1050.

[16] H. Li and Y. C. Shin, Analysis of bearing configuration effects on the high speed spindles using an integrated dynamic thermo-mechanical spindle model, *Int. J. Machine Tools Manufact.,* 44 (2004) 347-364.

[17] G. L. Xiong, J. M. Yi, C. Zeng, H. K. Guo and L. X. Li, Study of the gyroscopic effect of the spindle on the stability characteristics of the milling system, *Int. J. Machine Tools Manufact.,* 138 (2003) 379-384.

[18] V. Gagnol, B. C. Bouzgarrou, P. Ray and C. Barra, Model-based chatter stability prediction for high-speed spindles, *Int. J. Machine Tools Manufact.,* 47 (2007) 1176-1186.

[19] M. Bäker, Finite element simulation of high-speed cutting forces, *J. Mat. Proc. Tech.,* 176 (2006) 117-126.